Building and Environment, Vol. 24, No. 1, pp. 39–50, 1989.
Printed in Great Britain.

0360–1323/89 $3.00+0.00

#3335

Simulation of Wind Flow Around Three-Dimensional Buildings

D. A. PATERSON*
C. J. APELT†

In this paper results from a computer simulation of wind flows around prismatic bodies using a k–ε model of turbulence are compared with full scale and wind tunnel tests done by others. The agreement is good, both in the wake region and elsewhere, and is particularly good for flow around a cube in which the overall error level in both pressures and velocities is about 5–10%. This is comparable with the error achievable with well controlled wind tunnel tests.

NOMENCLATURE

b	breadth of building
C_P	pressure coefficient
c_μ, c_1, c_2	constants 0.09, 1.44, 1.92
H, h	height of building
k	turbulent kinetic energy
P	augmented pressure
$\bar{P}$	true mean pressure
P^*	production term in equations for turbulence quantities
S_C, S_P	source terms for differential equations
T	thickness of building
U, V, W	mean velocities along coordinate axes
U_i, U_j	mean velocities along coordinate axes
U_0	velocity in undisturbed flow at the same height
U_∞	velocity at the top of the boundary layer
U_r	reference velocity
U_τ, V_τ	friction velocities
u_i, u_j	fluctuating velocities
u_1, U_{rms}	fluctuating velocity in x direction
W, w	building half width
X, Y, Z	distances along coordinate axes
x, y, z	distances along coordinate axes
x_i, x_j	distances along coordinate axes
z	distance from solid surface
z_P	distance from reference point to solid surface
z_0	roughness length of solid surface

Greek symbols

Γ	general diffusion coefficient
γ	any large number (nominally infinite)
Δz	top of control volume next to a solid surface
δ	height of boundary layer
δ_{ij}	Kronecker delta
ε	dissipation of turbulent kinetic energy
κ	Kolmogoroff's constant, 0.4187
ν	kinematic viscosity of air
ν_t	turbulent kinematic viscosity
ρ	density of air
$\sigma_k, \sigma_\varepsilon$	constants 1.0, 1.3
ϕ	any convected quantity.

1. INTRODUCTION

THE PHENOMENA associated with wind flows around buildings and similar structures are of practical importance. Engineers and architects need to know the wind environment adjacent to the structure, the pressures on the cladding elements, the loads in the structural framework and the vibrations of the structure.

There are presently four main ways in which wind flow patterns around buildings and similar structures are found: from full scale tests, from wind tunnel tests, from calculations based on published data and from codes of practice. The aim of the present research is to develop and test a fifth way that has fewer drawbacks: computer modelling.

The results presented here are limited to the calculation of flows around single prismatic buildings on flat terrain and are limited to the calculation of mean and fluctuating velocities and mean pressures. However, programs have been written by the authors that can calculate flows over groups of buildings and over uneven terrain, and post-processing techniques have been developed that could be used to predict fluctuating pressures, loads and vibrations; these programs and techniques have not yet been properly tested.

2. EQUATIONS AND SOLUTION METHOD

The fundamental equations governing the motion of most fluids are the Navier–Stokes equation and the continuity equation. The steady-state Reynolds equation, which is presented below, is obtained by averaging the Navier–Stokes equation with respect to time.

$$U_j \frac{\partial U_i}{\partial x_j} = \frac{\partial}{\partial x_j}\left[\nu \frac{\partial U_i}{\partial x_j} - \frac{\bar{P}}{\rho}\delta_{ij} - \overline{u_i u_j}\right] \quad i = 1 \ldots 3, \quad (1)$$

where:

$\rho\overline{u_i u_j}$ is called the Reynolds stress tensor,

$$\delta_{ij} = \begin{cases} 1 & \text{if } i = j \\ 0 & \text{if } i \neq j. \end{cases}$$

The time averaged continuity equation is:

$$\frac{\partial U_j}{\partial x_j} = 0. \quad (2)$$

In these equations the convention of summation over repeated indices is used.

The Reynolds equation cannot be solved without first

* Department of Aeronautics, Imperial College, London SW7 2BY, U.K.
† Department of Civil Engineering, University of Queensland, St Lucia 4067, Australia.

introducing an approximation of the Reynolds stress tensor. The complete set of equations used in deriving this approximation is known as the turbulence model. For this study the k–ε model of turbulence was used. With this model, a system of six equations results. These equations are presented below.

$$U_j\frac{\partial k}{\partial x_j}=\frac{\partial}{\partial x_j}\left[\frac{\nu_t}{\sigma_k}\frac{\partial k}{\partial x_j}\right]+\nu_t\left[\frac{\partial U_i}{\partial x_j}+\frac{\partial U_j}{\partial x_i}\right]\frac{U_i}{\partial x_j}-\varepsilon,$$

$$U_j\frac{\partial \varepsilon}{\partial x_j}=\frac{\partial}{\partial x_j}\left[\frac{\nu_t}{\sigma_\varepsilon}\frac{\partial \varepsilon}{\partial x_j}\right]+c_1c_\mu k\left[\frac{\partial U_i}{\partial x_j}+\frac{\partial U_j}{\partial x_i}\right]\frac{\partial U_i}{\partial x_j}-c_2\frac{\varepsilon^2}{k}$$

$$U_j\frac{\partial U_i}{\partial x_j}=\frac{\partial}{\partial x_j}\left[\nu_t\frac{\partial U_i}{\partial x_j}\right]-\frac{\partial P}{\partial x_i}\quad i=1\ldots3$$

$$\frac{\partial U_j}{\partial x_j}=0 \tag{3}$$

where:

$\nu_t=c_\mu k^2/\varepsilon$	is the turbulent viscosity,
$P=\bar{P}/\rho+2k/3$	is the augmented pressure,
$k=\overline{u_ju_j}/2$	is the turbulent kinetic energy,
$\varepsilon=\nu\overline{(\partial u_i/\partial x_j)^2}$	is the turbulent energy dissipation.

These six equations are solved for six unknowns; the turbulent kinetic energy and its dissipation, the three mean velocity components and the augmented pressure.

An important analytical solution of these equations is an approximation to 3-D boundary layer flow given by:

$$U=\frac{U_\tau}{\kappa}\ln\frac{z}{z_0}\qquad V=\frac{V_\tau}{\kappa}\ln\frac{z}{z_0},$$

$$k=\frac{U_\tau^2+V_\tau^2}{\sqrt{c_\mu}}\qquad \varepsilon=\frac{(U_\tau^2+V_\tau^2)^{3/2}}{\kappa z},$$

$$\nu_t=c_\mu\frac{k^2}{\varepsilon}=(U_\tau^2+V_\tau^2)^{1/2}\kappa z\quad W=0. \tag{4}$$

In this solution the velocities parallel to a solid surface (U and V) are expressed as functions of the distance from that surface (z). The velocity perpendicular to the surface (W) is zero and the augmented pressure and the values U_τ, V_τ and z_0 are arbitrary constants. This solution is used both in determining initial conditions and in deriving boundary conditions.

Five of the six partial differential equations can be expressed in the following form:

$$U_j\frac{\partial\phi}{\partial x_j}=\frac{\partial}{\partial x_j}\left[\Gamma\frac{\partial\phi}{\partial x_j}\right]+S_C+S_P\phi \tag{5}$$

ϕ	Γ	S_C	S_P
U_i	ν_t	$-\dfrac{\partial P}{\partial x_i}$	0
k	$\dfrac{\nu_t}{\sigma_k}$	$\nu_t P^*$	$-\dfrac{\varepsilon}{k}$
ε	$\dfrac{\nu_t}{\sigma_\varepsilon}$	$c_1c_\mu kP^*$	$-c_2\dfrac{\varepsilon}{k}$

where:

$$P^*=\frac{\partial U_i}{\partial x_j}\left[\frac{\partial U_i}{\partial x_j}+\frac{\partial U_j}{\partial x_i}\right].$$

In this form these five equations can be discretized by use of the control volume technique in which the partial differential equations are integrated over appropriate control volumes on a staggered grid to obtain difference equations. In performing this integration hybrid upwind differencing was used. The method by which the pressure is calculated is known as SIMPLE (Semi-Implicit Method for Pressure Linked Equations) [1]. Algorithms SIMPLER and SIMPLEC [2] were tried and rejected [3].

The resulting algebraic equations were solved by a 3-D version of the ADI (Alternating Direction Implicit) procedure in which three sweeps of the solution domain (one in each of the coordinate directions) are done in each iteration.

Convergence was said to have been achieved when the final error (as calculated from the sum of the absolute values of the error at each node) in each of the six equations was less than two per cent of the initial error in that equation. This took about a hundred iterations and required about 15 c.p.u. minutes and 1 Mbyte of core storage on an IBM 3083E computer (at about 5 MIPS).

3. INITIAL AND BOUNDARY CONDITIONS

The grid and initial conditions are generated within the computer program. The grid is a staggered grid with intervals that expand in geometric progression away from building faces. The velocities are calculated at locations midway between the nodes where the pressure and turbulence quantities are calculated. The grid locations are found by an iterative procedure.

The initial approximation is found by combining the 3-D boundary layer flow described above and an axisymmetric potential flow field generated by a fluid source and a fluid sink. The purpose of this potential flow is to mimic the effect of the building on the far field flow so that the boundaries can be brought in close to the building without distorting the flow. To remove the singularities at the source and sink points the velocities are interpolated within the recirculation bubble in such a way that continuity is approximately conserved. The values of all variables on the fluid–fluid interfaces at great distances from the building are fixed at the values calculated by the initial approximation. On the symmetry plane of the flow the normal derivatives of all variables are set to zero (except for the normal velocity whose value is set to zero).

No boundary conditions are required for the pressure correction equation because the velocity components perpendicular to the boundary are given at each point on the boundary [1]. On solid surfaces the velocity components perpendicular to the boundary are set to zero.

Wall functions are based on the formulae given above for the 3-D boundary layer and are used in the prediction of turbulence quantities near, and velocities parallel to, solid surfaces. These wall functions are similar to those described elsewhere [4, 5] but are designed for 3-D rough wall constant density flow instead of 2-D smooth wall variable density flow. They have been developed as part of the current research effort.

In the control volume method the partial differential equations are integrated to get difference equations. Wall functions are derived by substituting integrals of the shear stress and turbulent energy dissipation derived from the 3-D boundary layer flow for the integrals that apply away from walls. This is equivalent to replacing the old values of the source terms in the equations by new values. Details of the derivation are given by Paterson [3]. The new values of the source terms are given by the following formulae. For the velocities parallel to the boundary:

$$S_P = S_P^{\text{old}} - c_\mu^{1/4} k^{1/2} \kappa (\ln \Delta z/z_0)^{-1} (\Delta z - z_0)^{-1}. \quad (6)$$

For the turbulent kinetic energy:

$$S_C = S_C^{\text{old}} - \nu_t \left[\frac{\partial U}{\partial z}\left[\frac{\partial U}{\partial z} + \frac{\partial W}{\partial x}\right] + \frac{\partial V}{\partial z}\left[\frac{\partial V}{\partial z} + \frac{\partial W}{\partial y}\right]\right]$$

$$+ c_\mu^{1/4} k^{1/2} \kappa (U^2 + V^2) \left[\ln \frac{\Delta z}{z_0}\right]\left[\ln \frac{z_P}{z_0}\right]^{-2} (\Delta z - z_0)^{-1},$$

$$S_P = S_P^{\text{old}} + \frac{\varepsilon}{k} - c_\mu^{3/4} k^{1/2} \left[\ln \frac{\Delta z}{z_0}\right] \kappa^{-1} (\Delta z - z_0)^{-1}. \quad (7)$$

For the dissipation of turbulent kinetic energy:

$$S_C = \gamma c_\mu^{3/4} k^{3/2} (\kappa z_P)^{-1},$$

$$S_P = -\gamma. \quad (8)$$

Inside the buildings new source terms are used to fix the values of each variable to the initial very small values. This has no effect on the convergence or accuracy of the solution but is done to stop underflow and overflow errors from occurring.

It was noted when running an early version of the program [6] that sometimes the flow did not separate at the front edges of the building and that when it did separate the size and strength of the recirculation bubble was too small. This problem was solved by changing the boundary conditions on the longitudinal velocity at nodes adjacent to the front edges of the building. A detailed view of the flow near such an edge is shown in Fig. 1a. The wall functions that are used elsewhere near solid surfaces cannot be applied to the calculation of the velocity at A. In the absence of more accurate information the value of the velocity at A was set to zero. This approximation has been used for three of the four flow cases described below. For the flow studied by Melbourne [7] and Holmes [8] the building is not a perfect prism;

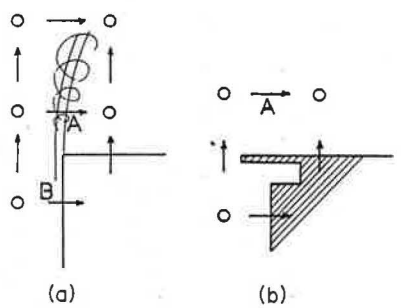

Fig. 1. (a) Details of the shear layer separating from the edge of a block. (b) Details of the top front edge of the Menzies building.

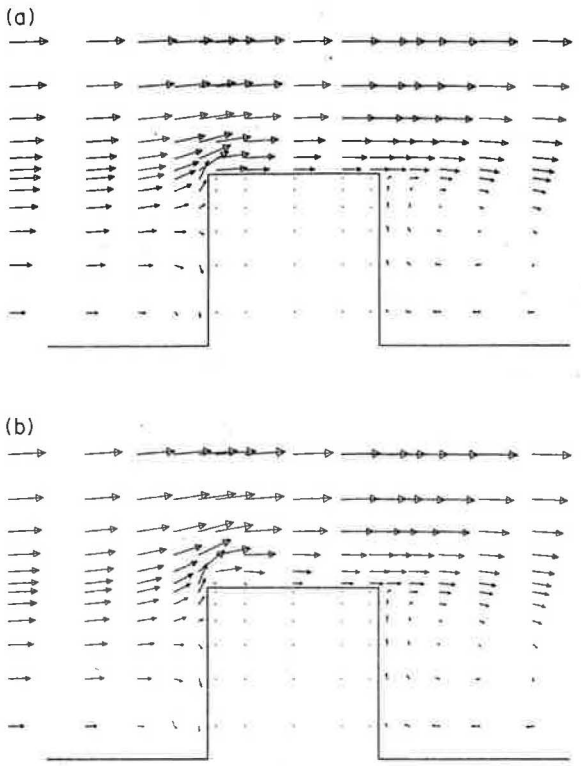

Fig. 2. Computed velocity vectors for flow over a cube: (a) using wall functions at the leading edge; (b) using a zero longitudinal velocity at the leading edge.

the top front edge has the configuration shown in Fig. 1b (drawn to scale) and the use of wall functions for the velocity at A is justified.

The effect of the velocity at A can be clearly seen in Fig. 2. The flow patterns here were observed on the plane of symmetry of the flow reported by Castro and Robins [9, 10]. The flow shown in Fig. 2a was computed using wall functions in the calculation of the longitudinal velocity adjacent to the front edge. The flow shown in Fig. 2b was computed with a zero longitudinal velocity adjacent to the front edge. The results shown in Fig. 2b agree very well with data inferred from [9, 10] and also agree very well with the results of a flow visualization study set up by the authors.

4. COMPARISON WITH EXPERIMENTS

Introduction

Five experimental studies of wind flows around isolated buildings were chosen for comparison with computations [3] and four are reported here. Comparisons of preliminary computations with three of these have already been reported [6]. These preliminary computations have been completely redone using better techniques. The experimental studies were chosen because they covered a wide range of width to height ratios and had results that could be easily compared with computed predictions.

Davies *et al.* [11] measured velocities in the near wake of a tall prism (Height : Width : Thickness = 6 : 1 : 1) in a wind tunnel using a pulsed wire anemometer. Results taken with the approach flow most nearly like the wind

profile in the open atmosphere were selected for comparison with computed predictions. Streamline patterns and r.m.s. velocity fluctuations were used as the basis for comparison.

Castro and Robins [9, 10] measured velocities and pressures in the vicinity of a 200 mm cube ($H:2W:T = 1:1:1$) in a wind tunnel. Velocities were measured using a pulsed wire anemometer. The results selected for comparison were taken from the measurements reported in both of the above references and were limited to the case with a turbulent boundary layer approach flow and where the front face was perpendicular to the approach flow direction. Mean pressures on the faces of the cube, mean velocities and turbulence intensities are compared with computed predictions.

A detailed study of velocities near prismatic obstructions in a wind tunnel was performed by Woo *et al.* [12]. Some of these results can also be found in a paper by Peterka and Cermak [13]. Results presented in both papers are compared with computed predictions in this report. Comparisons are made with measurements near a block $6.5 \times 15.9 \times 4.9$ cm ($H:2W:T = 1:2.4:0.75$) for the case where the approach flow is perpendicular to the front face of the block. Mean velocities and turbulence intensities are compared with computed predictions.

Measurements of mean wind pressures on the front and back faces of an isolated rectangular building, the Menzies building at Monash University, were reported by Melbourne [7]. The building is $43.2 \times 141 \times 12.9$ m ($H:2W:T = 1:3.3:0.3$). The pressures measured on the building surface were compared with pressures measured on a 1:600 scale model in a wind tunnel. Further measurements were reported by Holmes [8]. All sets of mean pressure measurements are compared with computed predictions in this report.

The coordinate system used in this report is shown in Fig. 3. This coordinate system differs from those used in some of the above papers.

There are difficulties in predicting the normal components of the Reynolds stress tensor. To avoid this problem in the following comparisons, measured values of $\overline{u_1 u_1}^{1/2}$ have been compared with computed values of $k^{1/2}$. For most flows described in this report the following relationship holds:

$$0.82k^{1/2} \leqslant \overline{u_1 u_1}^{1/2} < 1.41k^{1/2}. \qquad (9)$$

The lower limit implies homogeneous turbulence and the upper limit is approached in strongly sheared flows such as those very near solid surfaces.

In subsequent figures (except Figs 5, 6 and 12–15) the distance between adjacent symbols on the curves showing computed results is equal to the grid resolution. The pressures used in calculating pressure coefficients from computed results are not those on the exact surfaces of the buildings and blocks but are a half grid interval away from those surfaces. This leads to slight inaccuracies in regions where the pressure is varying rapidly and this should be taken into account when comparing computed and measured pressure coefficients.

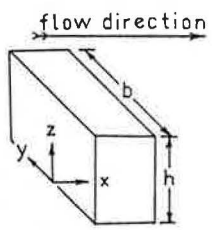

Fig. 3. Coordinate system.

Experiments by Davies et al. [11]

The approach velocity profiles of the computed and wind tunnel flows are shown in Fig. 4. Unfortunately, none of the three approach flows studied by Davies, Quincey and Tindall is similar to boundary layer flow in the open atmosphere. The approach flow with which a comparison was made is referred to as 'flow 2' in [11, Fig. 1]. All the velocity measurements by Davies *et al.* in the wake of the block were made using a pulsed wire anemometer which is claimed to give accurate results in flows of this type. The velocity profiles differ significantly for $30 < z < 170$ mm. The computed profile was based on a roughness length of 1.1 mm. It may be possible to get a better agreement using the power law profile option in the computer program.

Computed and measured streamlines in the wake of the block are shown in Fig. 5. The drawing in Fig. 5a is a photocopy of [11, Fig. 5] and the drawing in Fig. 5b was produced by a program written as part of the present research effort. The flow patterns are similar but not identical. The sizes of the rear recirculation region and the top recirculation region are smaller in the present computation, the height of the stagnation point is lower and the vertical component of the flow is smaller.

Profiles of the computed and measured velocity fluctuations behind the block are shown in Fig. 6. The measured velocity fluctuations are taken from [11, Fig. 2a]. Exact agreement between these profiles is not to be expected because different variables are being compared. This being so, the level of agreement obtained at heights below the height of the building is very good. The predicted magnitude of the velocity fluctuations at a height

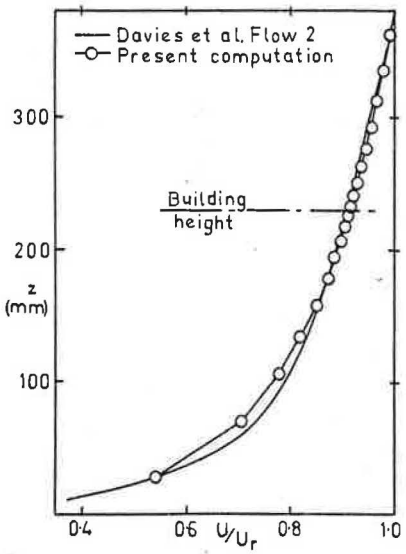

Fig. 4. Velocity profiles of approach flow for tall prism.

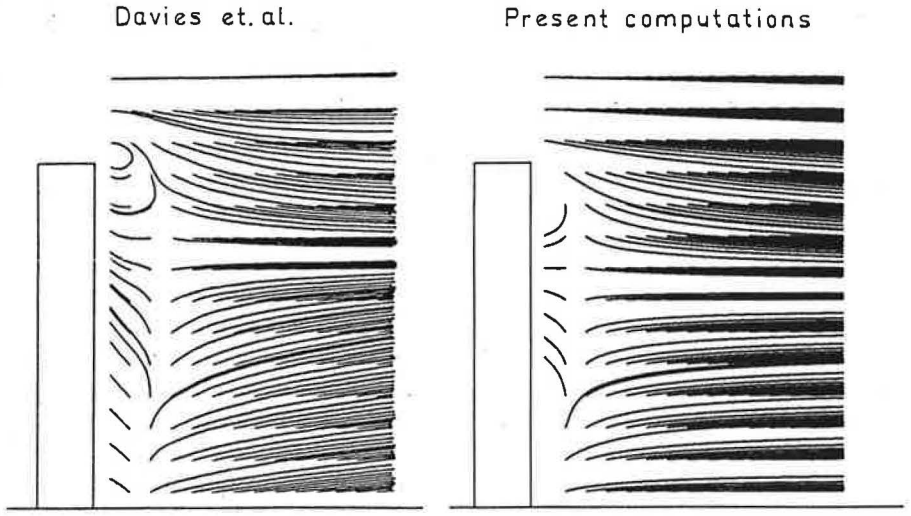

Fig. 5. Streamlines in the wake of the prism on the symmetry plane.

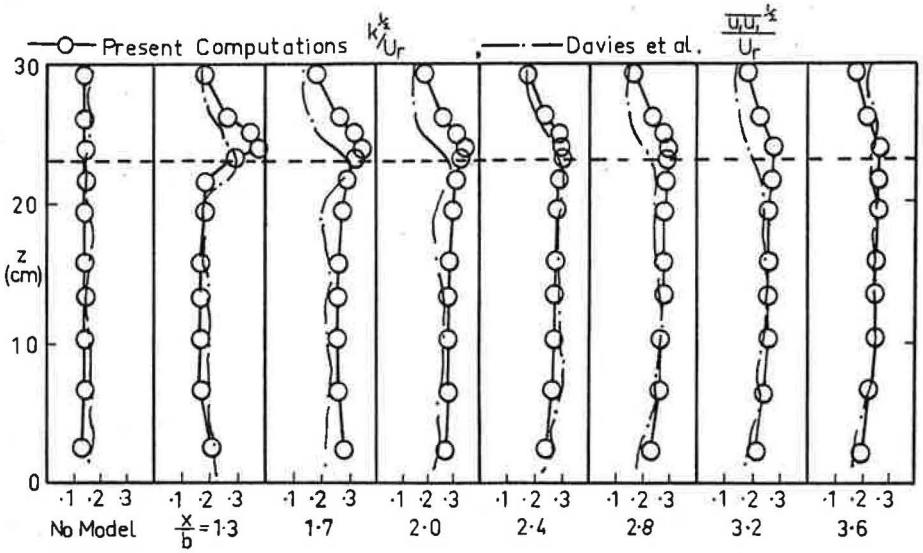

Fig. 6. Velocity fluctuations in the wake of the prism on the symmetry plane.

of about 1.1 times the building height seems to be slightly too large. Some of this discrepancy could be due to experimental inaccuracy; the reported values of the magnitude of the velocity fluctuations vary significantly, and in a random manner, between successive profiles.

Experiments by Castro and Robins [9, 10]

Comparisons of measured and computed coefficients of mean surface pressure on the cube are shown in Figs 7a and b. The measured pressure coefficients are taken from [9, Fig. 4], [10, Fig. 4]. The reference velocity for calculating these coefficients is taken as the velocity in the approach flow at a height equal to the height of the cube.

The overall agreement between the computed and the measured results is very good; the errors in the predicted pressures are typically about 10%. This is closer than the agreement between the three sets of wind tunnel results reported in Case A of [10, Fig. 4].

In Fig. 7a the agreement between the computed and measured pressures on the front and back faces of the cube is excellent and the agreement on the side and top faces of the cube is very good. In Fig. 7b some differences are noticeable. The computed prediction underestimates the pressures on the bottom of the front face and overestimates them at the top of the front face. Similar differences are evident on the side and back faces of the cube. The measured pressures on D differ between [9, 10]. The values from [10] are plotted here but those from [9] agree better with the computed values. The prediction of pressure on the top of the cube shows some areas of underprediction and some of overprediction.

Comparisons of measured and computed vertical profiles of longitudinal velocity above the cube and down-

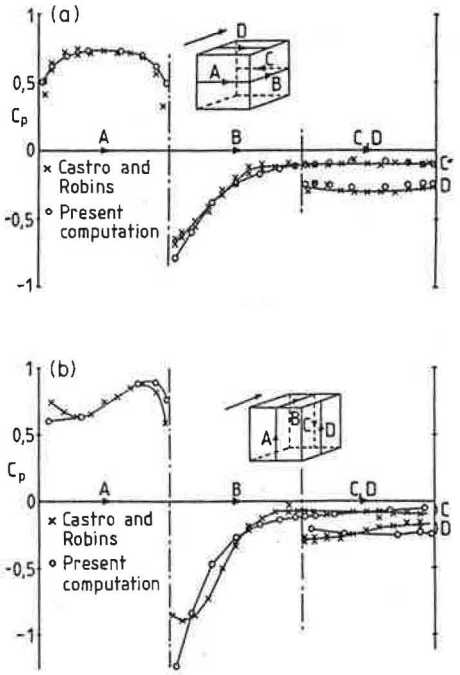

Fig. 7. Mean pressure coefficients on cube surface.

stream from it are shown in Fig. 8. The measured profiles are taken from [9, Figs 8, 10 and 12], [10, Fig. 6]. Castro and Robins have measured these velocities with a pulsed wire anemometer, which is claimed to give accurate results in such regions of flow. In the computation it has been assumed that the roughness length of the ground upstream of the cube is 4 mm and the roughness length of the cube surface is 0.04 mm.

As with pressure, the overall agreement is very good. The velocities are very well predicted at x/h values of 0.5 and 2.5. The location $x/h = 0.5$ is the centreline of the cube and not far downstream from the point of reattachment of the top recirculation region. The location $x/h = 1.5$ is only 100 mm downstream from the cube and the flow here is difficult to predict and difficult to measure, so the slight inaccuracies observed are not troublesome. The location $x/h = 2.5$ is near the point of reattachment of the main recirculation region and from this it can be seen that the computer prediction of the reattachment length is very good.

Measured and computed transverse profiles of longitudinal velocity behind the cube are shown in Fig. 9. The measured profiles are taken from [9, Figs 14 and 16], [10, Figs 8 and 9] and were taken at a height of $z/h = 0.5$.

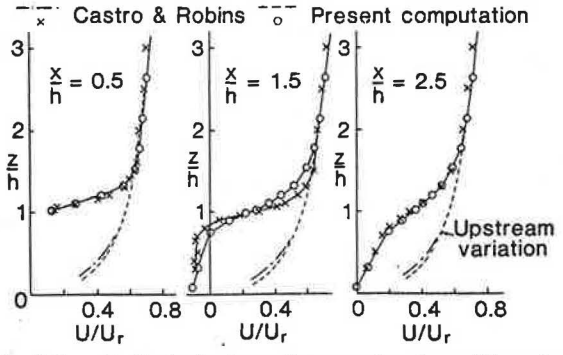

Fig. 8. Longitudinal velocity on the symmetry plane of the cube.

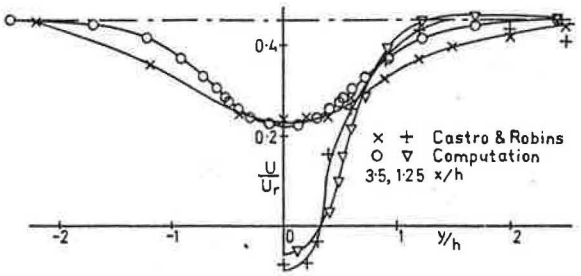

Fig. 9. Longitudinal velocity behind the cube at $z/h = 0.5$.

The agreement between the measured and computed profiles at $x/h = 1.25$ is fair but the two profiles differ significantly at $x/h = 3.5$. This difference is less than that observed in the earlier calculations [6] but is still significant. The reason for this difference is unknown; it is in the opposite direction to any possible error from numerical diffusion.

Measured and computed vertical profiles of the longitudinal velocity fluctuations are shown in Fig. 10. The measured profiles are taken from [9, Figs 9, 11 and 13], [10, Fig. 7]. Exact agreement between the measured and computed profiles is not to be expected for two reasons: the magnitude of the velocity fluctuations upstream from the cube in the wind tunnel study is very different from that in the computer study; and the variables that are compared are different and the best that can be expected is given in Equation (9). However, even allowing for these, the computed peak value of turbulence is too small and dies away too rapidly with distance downstream.

Experiments by Woo, Peterka and Cermak [12, 13]

A large number of measurements were taken by Woo, Peterka and Cermak of wind tunnel flows around rectangular blocks [12, 13]. Only those that are also reported in [13] have been used for comparison with predictions by the present computer program. In computations, the surface of the block was assumed to have a roughness length of 0.04 mm and the ground a roughness length of 1.5 mm.

Profiles of the mean velocity and of the turbulence intensity in the approach flow are shown in Fig. 11. The measured values are taken from [12, Fig. 2], [13, Fig. 3]. The profile of the turbulence intensity reported by Woo *et al.* is different from that reported by Peterka and Cermak. In a private communication, Peterka has said that the results reported by Woo *et al.* are probably more accurate. For the present computation, the values of

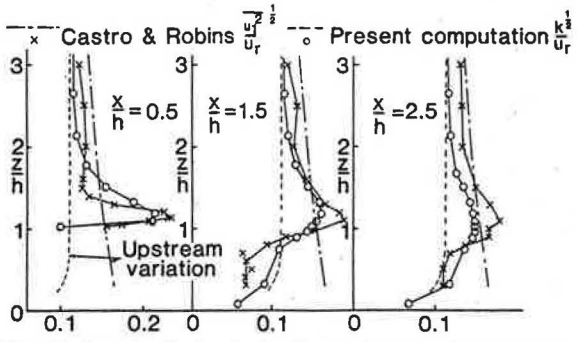

Fig. 10. Longitudinal velocity fluctuations on the symmetry plane of the cube.

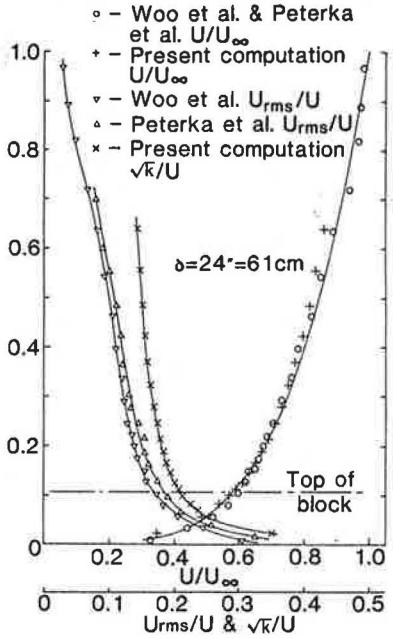

Fig. 11. Mean velocity and turbulence intensity in the approach flow.

different variables are plotted and so exact agreement with the wind tunnel measurements is not to be expected. If the computed values were 10% less over the whole height of the flow then the agreement with the measured intensity would be excellent.

Vertical and transverse profiles of the mean velocity deficit behind the block are shown in Figs 12 and 14. The measured values are taken from [12, Figs 34 and 36], [13, Figs 4 and 6]. The values of x/h on these graphs are calculated with $x = 0$ at the back face of the block; the vertical profiles are taken on the plane of symmetry of the flow ($y = 0$) and the transverse profiles are taken at a height of $z/h = 0.8$. A large amount of post-processing of the computer output was required because the original wind tunnel measurements were taken with a single wire hot film anemometer.

For the vertical profiles in Fig. 12 the agreement is good. For $x/h > 0.5$ the computed prediction of the velocity deficit is too large for $z/h < 1$ and too small for $1.5 < z/h < 3$. The reason for this discrepancy is unknown. For the transverse profiles of the mean velocity deficit the agreement is reasonable. At $x/h = 1$ the post-processing of output near the centreline produced physically impossible results which were not plotted. For $x/h > 3$ there are regions where the computed prediction of the velocity deficit is too large near the centreline and too small at larger values of y/w.

Vertical and transverse profiles of the turbulence intensity excess are shown in Figs 13 and 15. The measured values are taken from [12, Figs 35 and 37], [13, Figs 5 and 7]. A large amount of post-processing of the computer output was required. The values of x/h on these graphs are calculated with $x = 0$ at the back face of the block; the vertical profiles are taken on the plane of symmetry of the flow ($y = 0$) and the transverse profiles are taken at a height of $z/h = 0.8$. At many locations the post-processing produced physically impossible results which were not plotted. The irregular shapes of the predicted profiles with $x/h < 4$ are probably due to the inaccuracy of the post-processing procedure. As before, there are regions where the computed predictions are too large (near the ground and near the plane of symmetry) and regions where the computed predictions are too small (at z/h about 2 and $2y/w$ about 2).

Experiments by Melbourne [7] *and Holmes* [8]

Melbourne [7] reported measurements of pressures on the Menzies building at Monash University. Later measurements of pressures were reported by Holmes [8]. A sketch of this building showing surrounding buildings is given in Fig. 16. This building is isolated and was modelled on the computer as a rectangular block. In the computer model the service penthouse, the ground floor veranda in front of the building, and the ground floor projections behind the building were ignored. The building surface roughness was assumed to be isotropic with a roughness length of 1 cm.

Melbourne has not reported measurements of the wind velocity in the open atmosphere in the approach flow to the Menzies building but has reported the equivalent measurements taken in wind tunnel studies. A comparison of the approach velocity profile of the present computer simulation with two profiles measured by Melbourne in the wind tunnel studies is shown in Fig. 17. The good agreement is not surprising; the computer program allows the user to select the position and slope of the line on this graph. The roughness length of the ground upstream of the building in the computer study was assumed to be 1 m. This becomes 1/6 cm when translated to the model scale of 1 : 600.

Comparisons of the velocity fluctuations in the approach flows in the wind tunnel studies with those in the present computer simulation are shown in Fig. 18. Because different variables are plotted for the different studies exact agreement is not to be expected. The level of agreement achieved is satisfactory for heights less than 1.6 times the building height.

Comparisons of wind tunnel, full scale and computed pressures are shown in Fig. 19 and Table 1. Figure 19 is analogous to [7, Fig. 5] and Table 1 is analogous to Tables 1 and 2 in [8]. The wind tunnel results correspond to the "3 cm roughness Menzies building alone" flow case reported by Melbourne. The full scale readings by Melbourne are the averages of four separate readings within a ten minute interval. The full scale readings by Holmes are averages over 15 min. The reference velocity for the calculation of the pressure coefficients is taken as the velocity in the approach flow at the height of the building. In obtaining computer predictions the heights of floors 4, 8 and 10 have been assumed to be 19, 33 and 40 m respectively. These could be in error by up to one metre.

In Fig. 19 the vertical bars on the full scale results by Melbourne represent the standard deviation of the four readings that were taken, averaged over the five values on each floor on each face. The computed results agree well with both the wind tunnel and full scale results on floor 8 of the front face of the building. On the back face the computed results also agree well with wind tunnel results but the agreement of both with the full scale results is not as good. This could be because the full scale

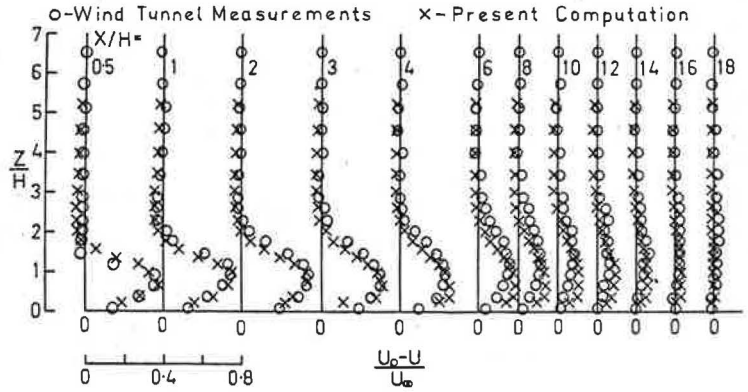

Fig. 12. Mean velocity deficit on the symmetry plane.

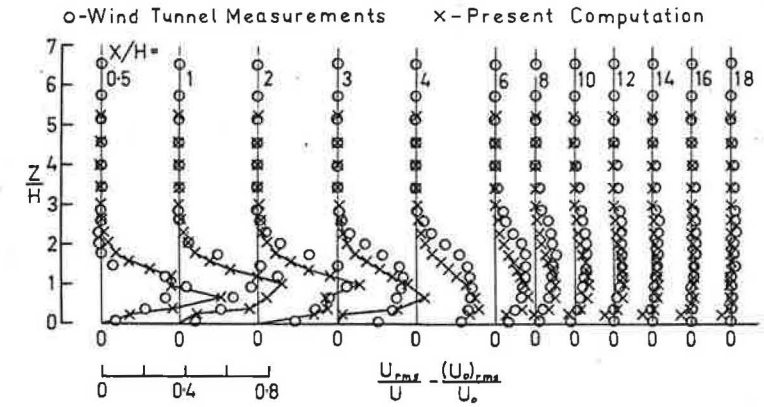

Fig. 13. Turbulence intensity excess on the symmetry plane.

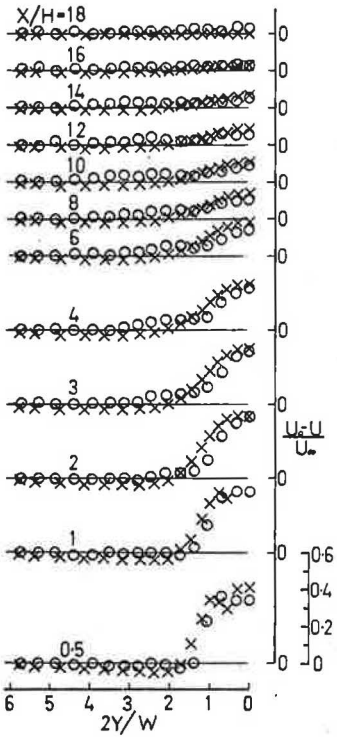

Fig. 14. Mean velocity deficit at $z/h = 0.8$.

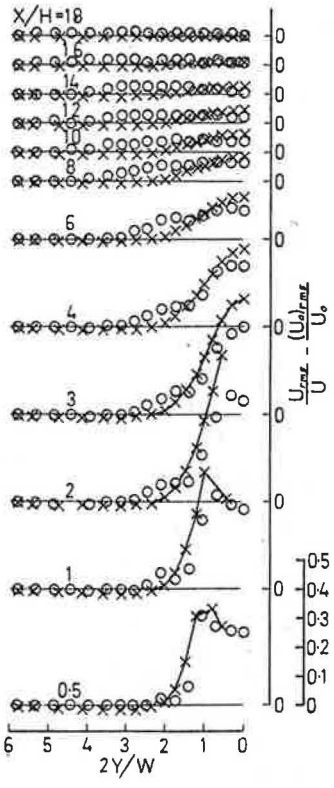

Fig. 15. Turbulence intensity excess at $z/h = 0.8$.

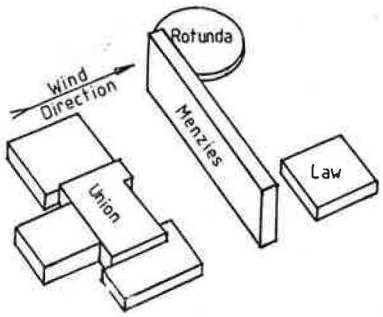

Fig. 16. The Menzies building and surrounding buildings.

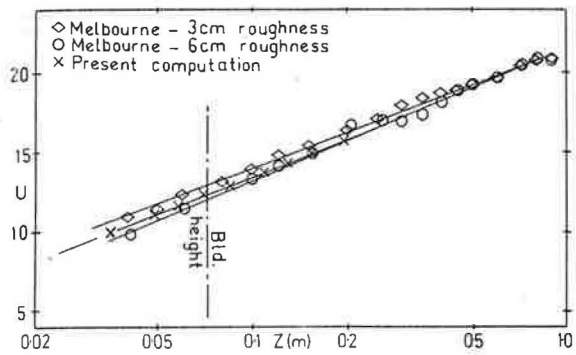

Fig. 17. Velocity profiles of flow approaching the Menzies building.

measurements are not true mean pressures but short term averages; it could also be partly due to the lack of detailed knowledge of the approach wind conditions in the full scale flow. On floor 10 of the front face the computed pressures appear to be too small for y/b less than 0.4. Floor 10 is near the top of the building and the pressure is varying rapidly with height at this level.

On floor 4 of the front face the computed results agree reasonably well with the full scale measurements but not as well with the wind tunnel measurements. At this height the pressures measured in the wind tunnel are much less than on floor 8, which suggests that the wind tunnel readings may be in error because other wind tunnel and full scale studies report large pressure coefficients at a height corresponding to floor 4. The comparisons in Table 1 tend to confirm the conclusions drawn from Fig. 19. For the first five of the C_P values from Holmes, errors of the order 0.2 can be expected because of zero drift in both the transducer and the carrier amplifier units; this was corrected for the last two C_P values and it can be seen that the agreement between the full scale, wind tunnel and

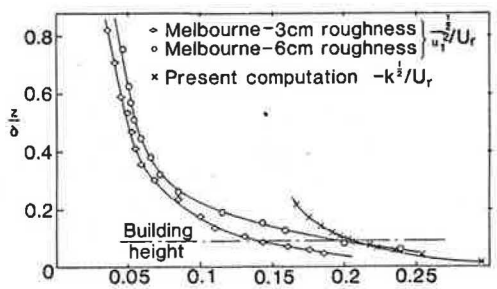

Fig. 18. Velocity fluctuations in flow approaching the Menzies building.

computed pressures for these two C_P values is quite good. The errors of order 0.2 also apply to the full scale results by Holmes plotted on Fig. 19.

Overall, the computed results agree well with the wind tunnel measurements. The difference between the computed results and the wind tunnel measurements is less than that between the different wind tunnel measurements reported in [7, Fig. 5]. The agreement with the full scale measurements is not as good.

Summary of comparisons

In general, the agreement between the computed results and the results of experiments performed by others is very good for the flows measured by Castro and Robins and by Melbourne and good for the flows measured by Davies *et al.* and by Woo *et al.*

For the flow measured by Davies *et al.*, there is a good qualitative agreement between the computed and measured streamline patterns on the symmetry plane of the flow in the wake of the block but three differences have been noted. The computed predictions of the velocity fluctuations in the wake agree to within experimental accuracy with the wind tunnel measurements at heights less than the building height and there are only slight differences above that height.

For the flow measured by Castro and Robins the pressures on all faces of the cube are very well predicted. The longitudinal velocities above and in the near wake of the cube are also very well predicted (but the predicted transverse profile of the longitudinal velocity at $x/h = 3.5$ is not very accurate). The predictions of the velocity fluctuations above and behind the cube are as good as can be expected.

For the flow measured by Woo *et al.* the mean velocity deficit and turbulence intensity excess in the wake of the block are compared with predictions. Overall the agreement is good. There are some differences due to problems with the post-processing scheme used. There is also some overestimation of these quantities near the ground and the plane of symmetry and some underestimation elsewhere.

For the flow measured by Melbourne the computed pressures on the front and rear faces of the building agree very well with those measured in the wind tunnel study. The only substantial differences are on floor 4 of the front face where the predicted pressures are too high and on floor 10 of the front face where the predicted pressures are too low. The full scale readings differ from both the wind tunnel and computed predictions and reasons for this are given.

Overall, the accuracy of the present computations is not much less than that obtained by well set up wind tunnel tests. The accuracy presently obtained is also better than that which has been previously obtained with computer modelling.

5. COMPARISON OF CALCULATED FLOW FIELDS

Plots of streamlines of mean velocity fields are useful as a tool for visualizing the 3-D flow patterns. From them it is relatively easy to see the shape and size of recirculation regions. They should be treated with

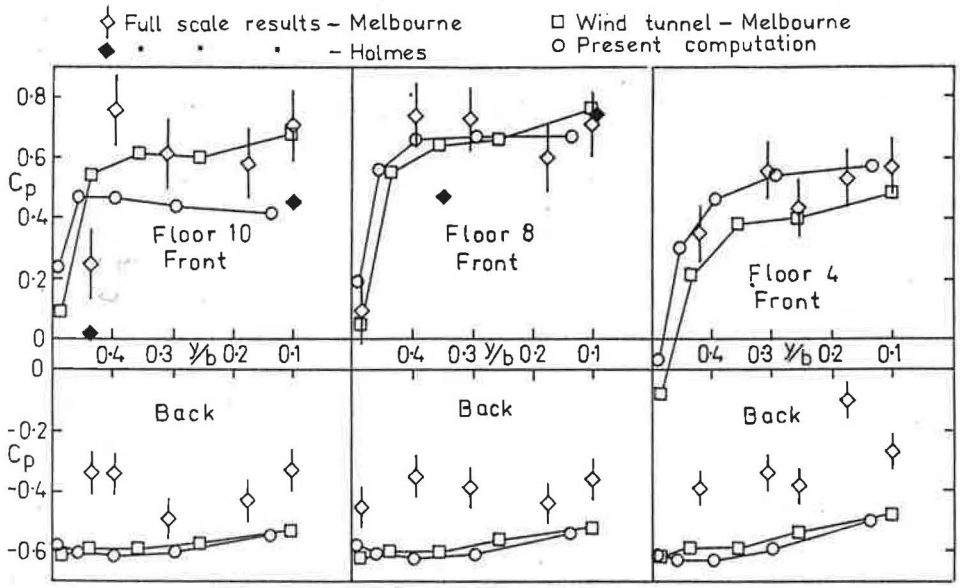

Fig. 19. Pressure coefficients on the Menzies building.

Table 1. Pressure coefficients on the Menzies building

Face	Front	Front	Front	Front	Front	Front	Back
Height (m)	40	33	26	40	33	36.5	36.5
Distance from centre (m)	60	49	49	13	13	49	49
Full scale* C_P	0.02	0.47	0.04	0.45	0.74	0.62	−0.50
Full scale† C_P	0.25	—	—	0.67	0.71	—	—
Computation C_P	0.47	0.66	0.59	0.42	0.67	0.64	−0.61
Wind tunnel C_P	0.54	0.64	0.56	0.68	0.76	0.66	−0.58

* Holmes.
† Melbourne.

caution, however, for two reasons. First, the patterns can depend significantly on the interpolation techniques used, particularly in the near wall regions. Second, because of turbulence actual particles in the flow will not follow the mean streamlines and this makes the shapes of the streamlines difficult to confirm by experimental observations. However, the mean streamline patterns presented here have in general been confirmed in flow visualization studies.

In the figures presented in this section only half the flow fields are drawn because the mean flow fields are symmetric (this would even apply if vortex shedding was present). The mean streamlines are considered to be traversed by fictitious particles. (If the flow was laminar then these would be actual fluid particles.) The flow direction is from left to right.

Two views of the computed flow corresponding to a flow measured by Davies *et al.* [11] are shown in Fig. 20. The lines in this and subsequent figures are streamlines of the time averaged flow field. From this figure it can be seen that there is a small recirculation region behind the block. Any fictitious particles released at a low level near the downstream edge of this recirculation region move first towards the symmetry plane of the flow then towards the building and away from the symmetry plane in a spiral motion, gradually gaining in height. As they gain

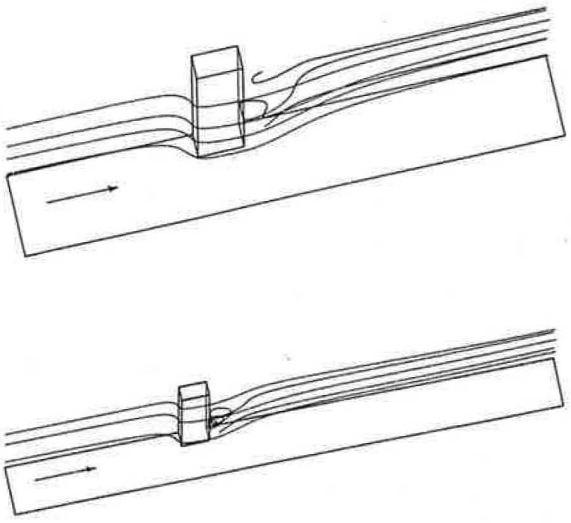

Fig. 20. Mean streamlines in flow over the tall prism.

in height the spiral expands and the particles eventually leave the recirculation region at the side of the block.

The mean streamlines do not form closed loops in recirculation regions in 3-D flow (as they would in 2-D flow). For this flow mean streamlines enter the region at

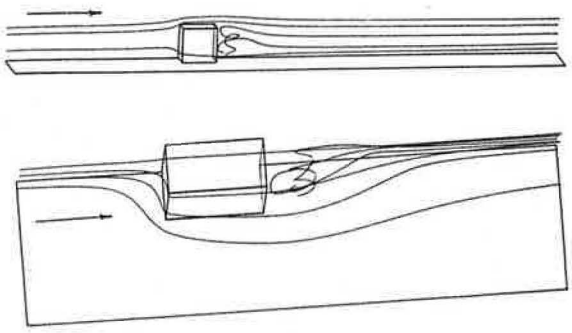

Fig. 21. Mean streamlines in flow over the cube.

the side of the block near the ground and at the top of the block near the plane of symmetry.

Two views of the computed flow corresponding to the flow measured by Castro and Robins [9, 10] are shown in Fig. 21. There are certain resemblances between the recirculation region behind this cube and that behind the tall prism used by Davies *et al.*; some fictitious particles released at a low level in the rear recirculation region travel in a spiral motion, gradually gaining in height. This spiral, however, starts at the side of the cube and ends at the top near the symmetry plane of the flow. A particle released near the ground and the symmetry plane is swept towards the cube and then outwards and upwards to leave the recirculation region about half way up the side of the cube.

From other mean streamline plots (not shown here) it can be seen that the recirculation region on top of the cube is small and streamlines pass forwards and backwards within it many times before leaving. The recirculation region beside the cube is wide near the ground and narrows towards the top and streamlines spiral rapidly upwards within it. The recirculation region in front of the cube is characterised by a downwards flow on the front face and a flow away from the cube near the ground but there is no indication (at this grid resolution with these boundary conditions) of the formation of a horseshoe vortex. Streamlines that pass through the front recirculation region also sometimes pass into the side or rear recirculation regions.

Two views of the computed flow corresponding to the flow measured by Woo, Peterka and Cermak [12, 13] are shown in Fig. 22. As in the computed flow corresponding to the flow measured by Castro and Robins a fictitious particle released in the rear recirculation region near the ground and the symmetry plane is swept towards the block and then outwards and upwards. It leaves the recirculation region near the top side corner of the block. Again spiralling motion is seen but the spirals are wider, longer and flatter than those in the flow around a cube.

Two views of the computed flow corresponding to the flow measured by Melbourne [7] and Holmes [8] are shown in Fig. 23. The spiralling motion is much longer and flatter than in the other flows. In this figure a mean streamline starts upstream of the block, passes around the edge of the block and enters the rear recirculation region. It is swept towards the block and then upwards, and leaves the recirculation region at the top.

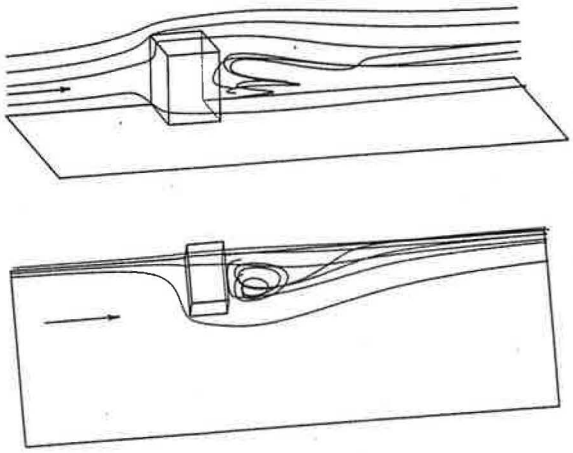

Fig. 22. Mean streamlines in flow corresponding to that in [12, 13].

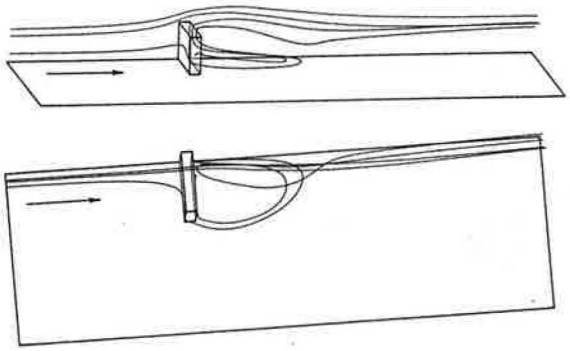

Fig. 23. Mean streamlines in flow over the Menzies building.

6. CONCLUSIONS

In this paper results from a computer program developed by the authors have been compared with results from both wind tunnel and full scale tests done by others. The overall agreement is very good, about as good as could be achieved by well controlled wind tunnel tests. The program has been written so that it can be used by any competent engineer or architect to determine wind velocities and pressures in the vicinity of single isolated buildings with one face perpendicular to the approach flow direction. It has now been developed to a stage where it could be used for research and is also ready for use in the preparation of tables and graphs for use in design. It is not yet ready, however, to be used as replacement for wind tunnel tests in the detailed design of individual buildings.

The results presented here are limited to the calculation of flows around single prismatic buildings on flat terrain and are limited to the calculation of mean and fluctuating velocities and mean pressures. However, programs have been written by the authors that can calculate flows over groups of buildings and over uneven terrain, and post-processing techniques have been developed that could be used to predict fluctuating pressures, loads and vibrations; these programs and techniques have not yet been properly tested.

REFERENCES

1. S. V. Patankar, *Numerical Heat Transfer and Fluid Flow*, McGraw-Hill, New York (1980).
2. J. P. Van Doormal and G. D. Raithby, Enhancements of the SIMPLE method for predicting incompressible flows. *Numerical Heat Transfer* 7, 147–163 (1984).
3. D. A. Paterson, Computation of wind flows over three-dimensional buildings. PhD Thesis, University of Queensland, Brisbane (1986).
4. B. E. Launder and D. B. Spalding, The numerical computation of turbulent flows. *Comput. Methods Appl. Mech. Engng* 3, 269–289 (1974).
5. A. D. Gosman and F. J. K. Ideriah, TEACH-T: A general computer program for two-dimensional turbulent recirculating flows. Dept. of Mech. Engng, Imperial College, London (1976).
6. D. A. Paterson and C. J. Apelt, Computation of wind flows over three-dimensional buildings, *J. Wind Engng Ind. Aerodyn.* **24**, 193–213 (1986).
7. W. H. Melbourne, Comparison of pressure measurements made on a large isolated building in full and model scale. Proceedings of the 3rd International Conference on Wind Effects on Buildings and Structures, p. 253. Saikan Shuppan, Tokyo (1971).
8. J. D. Holmes, Pressure fluctuations on a large building and alongwind structural loading. *J. Ind. Aerodyn.* **1**, 249–278 (1976).
9. I. P. Castro and A. G. Robins, The effect of a thick incident boundary layer on the flow around a small surface mounted cube. R/M/N795, Central Electricity Generating Board, Marchwood (1975).
10. I. P. Castro and A. G. Robins, The flow around a surface mounted cube in uniform and turbulent streams. *J. Fluid Mech.* **79**, 307–336 (1977).
11. M. E. Davies, V. G. Quincey and S. J. Tindall, The near wake of a tall block in uniform and turbulent flows, in *Wind Engineering* (Edited by J. E. Cermak), p. 289. Pergamon Press, New York (1980).
12. H. G. C. Woo, J. A. Peterka and J. E. Cermak, Wind tunnel measurements in the wakes of structures. NASA-CR-2806, N77-19716 (1977).
13. J. A. Peterka and J. E. Cermak, Turbulence in building wakes. Proceedings of the 4th International Conference on Wind Effects on Buildings and Structures, p. 447. Cambridge University Press (1977).